

COMPUTATIONAL AND EXPERIMENTAL INVESTIGATION OF THE BREAKUP MECHANISM OF BUBBLES AND DROPS IN TURBULENT FLOWS

Ronnie ANDERSSON^{1*} and Arash HELMI²

¹ Department of Chemical and Biological Engineering, Chalmers University of Technology, SE-41296 Gothenburg, Sweden

² Department of Chemical Engineering and Chemistry, Eindhoven University of Technology, 5600 MB Eindhoven, The Netherlands

*Corresponding author, E-mail address: ronnie.andersson@chalmers.se

ABSTRACT

This work focuses on understanding the breakup mechanism of bubbles and drops in turbulent multiphase flow. For this purpose CFD simulations based on a combination of large eddy simulations (LES) and volume of fluid (VOF) are validated using high speed camera measurement of the breakup dynamics. Very good agreement was found, both for deformation time and length scales and for the resulting size of the daughter fragments. The analysis reveals that eddies larger than the fluid particles also contribute to the breakup. It was also observed that the axis of the deformed particle and the vortex core axis were aligned perpendicular to each other, and that the breakup can sometimes occur due to interaction with two eddies at the same time. In these cases the vortex core axes were also aligned perpendicular. This means that more energy will be available and that the breakup rate will be affected.

NOMENCLATURE

A	interfacial area
C	phase function
d	fluid particle diameter
\mathbf{F}_i	interfacial tension force
g	gravity
p	pressure
\mathbf{S}	strain rate
\mathbf{u}	velocity
γ	normalized interfacial energy
κ	curvature
ρ	density
μ	dynamic viscosity
σ	interfacial tension
Ω	rotation rate

Subscripts

c	continuous phase
d	dispersed phase

INTRODUCTION

Multiphase flows are frequently encountered in the chemical and process industries. One critical part in the design and operation of multiphase flow processes is the

prediction of the dispersed phase size distribution. The mathematical framework needed to predict size distributions using CFD and population balance modelling is well established and the algorithms are now included in commercial codes. However, the accuracy of the prediction relies on the validity of the models used for the breakage and coalescence rates (Andersson et al., 2004). These two phenomena have been studied for more than fifty years, and a numerous models have been proposed. Liao and Lucas have recently reviewed breakup and coalescence rates models for turbulent flows (Liao and Lucas, 2009, Liao and Lucas, 2010).

A few years ago the authors presented high resolved measurements of single fluid particle breakup which showed that the breakup occurs within a few milliseconds (Andersson and Andersson, 2006b). The short breakup time scale, comparable to the lifetime of the vortices and the structured deformation indicates that breakup occurs due to interaction with single turbulent vortices. Hence, this phenomenon should be described as an interaction between fluid particles and individual turbulent structures. It should not be seen as interaction with the averaged properties of the turbulent structures.

Further it is important to know the range of vortices that contribute to the breakup rate. Currently there is no consensus in the literature if eddies larger than fluid particle contribute to breakup. Some of the most popular models in the literature assume that only eddies smaller and equal to the size of the fluid particles contribute to the breakup. It has been shown that relaxing this criteria in these models, causes a drastic increase in the predicted breakup rates. Consequently if eddies similar in size or somewhat larger also contribute the assumptions in these models are wrong.

In this work we assess if CFD simulations can be used as a tool to study the fundamental mechanisms behind gas bubble and droplet breakup in turbulent flows. Such an approach requires that the model resolves the disruptive and cohesive stresses accurately. The model must allow analysis of how the fluid particle interact with turbulent vortices during breakup. Several important questions must be addressed, among these we focus on the following two: Does breakup occur due to interaction with one or more eddies? How large are the vortices that cause breakage?

VOF simulations are extensively used to simulate multiphase flows. Li and co-workers simulated the breakup of viscous drops, subjected to shearing between

parallel plates under laminar conditions (Li et al., 2000). The volume of fluid model was also used by Lubin who studied air entrainment in breaking waves by using a combination of VOF and large eddy simulations (Lubin et al., 2006). A combination of LES and VOF was also used by Lacanette and coworkers to investigate hydrodynamic coating techniques (Lacanette et al., 2006). Shinjo and Umemura studied the disintegration of high-speed liquid jets injected into stagnant air by using direct numerical simulations (Shinjo and Umemura, 2010).

Based on the requirement the model should capture the essential physics; a combination of large eddy simulations (LES) and volume of fluid (VOF) simulations is used in this study.

MODEL DESCRIPTION

Breakup of fluid particles occurs when the disruptive stresses exceeds the cohesive interfacial stress. By using LES the large and intermediate turbulent vortices are resolved and only the smallest vortices are filtered out. The cohesive interfacial stress is predicted using a continuum interface force model. It is expected that a dense mesh at the interface region is needed to resolve the local curvature that causes the cohesive stress.

Governing equations

This work is limited to incompressible two-phase flow with constant interfacial tension. The flow consists of two immiscible fluids with different viscosities and densities. The flow is thus modelled by the spatially filtered Navier-Stokes equations

$$\nabla \cdot \bar{\mathbf{u}} = 0 \quad (1)$$

$$\rho \left(\frac{\partial \bar{\mathbf{u}}}{\partial t} + \bar{\mathbf{u}} \cdot \nabla \bar{\mathbf{u}} \right) = -\nabla \bar{p} + \rho \mathbf{g} + \nabla \cdot \left[(\mu + \mu_T) (\nabla \bar{\mathbf{u}} + \nabla^T \bar{\mathbf{u}}) \right] + \mathbf{F}_i \quad (2)$$

where \mathbf{g} is the gravity vector, μ_T is the subgrid scale turbulent viscosity, and \mathbf{F}_i is the source term in the momentum equation that accounts for the interfacial tension force.

Since the two fluids are not interpenetrating the instantaneous location of the two fluids is represented by the phase function $C(\mathbf{x},t)$, which takes the value one for the continuous phase and the value zero for the dispersed phase. The phase function, $C(\mathbf{x},t)$, which characterizes the topological changes of the interface is governed by an advection equation

$$\frac{\partial C}{\partial t} + \bar{\mathbf{u}} \cdot \nabla C = 0 \quad (3)$$

The model is closed by calculating the average values of the density and viscosity

$$\rho = C\rho_1 + (1-C)\rho_2 \quad (4)$$

$$\mu = C\mu_1 + (1-C)\mu_2 \quad (5)$$

In Eqs. (4) and (5), the subscripts 1 and 2 refers to the two different phases. Further the phase function allows the interface to be identified, by calculating the iso-surface of $C=0.5$ at each time step. The interfacial area is continuously changing due to the deforming stresses, but this can be quantified at each time by integrating the iso- C surface.

Interfacial tension

The interfacial tension forces, \mathbf{F}_i , caused by the interfacial tension, σ , are accounted for as a source term in the momentum Eq. (2). The source is calculated from the gradient of the local volume fraction (Brackbill et al., 1992) i.e. it is calculated from the phase function. The interfacial tension force is given by

$$\mathbf{F}_i = \sigma \kappa \mathbf{n}_s \delta_i = \sigma \nabla \cdot \left(\frac{\nabla C}{\|\nabla C\|} \right) \cdot \nabla C \quad (6)$$

where κ is the curvature and \mathbf{n}_s is the normal vector to the interface. The normal vector and the curvature are determined from the gradients of the phase function $C(\mathbf{x},t)$.

Turbulence model

By using large eddy simulation all the turbulent structures except the smallest scales are resolved. The scale separation is carried out through the spatial filtering implied by the computational grid, and the effect of the small unresolved scales are modelled using a subgrid viscosity μ_T Eq (2). In this study the dynamic Smagorinsky-Lilly model was used (Lilly, 1992).

Numerical methods

The governing equations are solved by using the finite volume method on a hexahedral mesh and by using a dynamic grid refinement that at each time step, locally refines the mesh at the interface. In zones behind the fluid particle the mesh is coarsened to its original mesh resolution to comply with LES standards.

Identification of turbulent vortices

In order to visualise the turbulent vortices the second invariant of $\nabla \mathbf{u}$ (or the Q-criterion) is used, it represents the local balance between rotation rate and strain rate (Hunt, 1987).

$$Q = \frac{1}{2} \left(|\boldsymbol{\Omega}|^2 - |\mathbf{S}|^2 \right) \quad (7)$$

Regions dominated by vorticity, where $Q > 0$, are defined as vortices.

EXPERIMENTAL METHOD

The experimental setup includes a flow reactor with mixing plates as shown in Figure 1. Compared to other reactors, e.g. stirred tank reactors, this reactor produces very homogeneous turbulence by continuous production and dissipation of turbulence in each mixing element. In addition, a major advantage of performing these measurements in this system is that turbulence is high at moderate bulk Reynolds number, which means that relatively low linear velocities can be used, which significantly simplifies obtaining sharp pictures of these fast phenomena. Nonetheless very strong light sources must be used to allow short exposure time. The data sampling rate, up to 4000 Hz, is enough to resolve the dynamics of these phenomena for all flow conditions. A more detailed description of the experimental system is found in the literature (Andersson and Andersson, 2006b). Detailed characterization of the single phase flow and turbulence through PIV measurements in these mixing elements is given by Bouaifi et al. (Bouaifi et al., 2004). In this study water is used as the continuous phase and the dispersed phase used is dodecane, its properties are $\rho=750$ kg/m³, $\mu_d=0.0015$ [Pas] and the interfacial tension $\sigma=0.053$ [N/m]. In this study no mass transfer and no chemical reactions occur that affect the flow. By introducing single drops the hold-up of the dispersed phase is negligibly low and the turbulence in the bulk will not be modulated due to this.

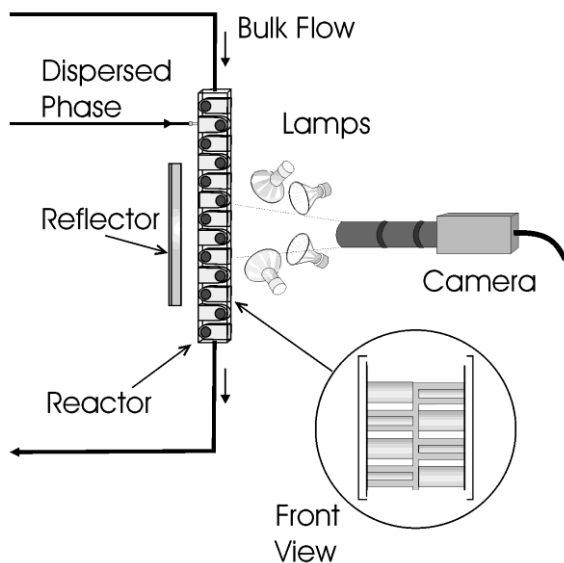


Figure 1: Experimental setup for high-speed video imaging, auxiliary pumps and data acquisition are excluded from the schematic figure.

RESULTS AND DISCUSSION

Using large eddy simulations the large and intermediate vortices are resolved directly while the effect of the smallest vortices are modelled. In Figure 2 the turbulent vortices are visualized by using the iso-Q criterion coloured with the vorticity magnitude. Here the maximum vorticity equals 3000 s⁻¹. In these large eddy simulations the grid resolution was determined from the Taylor micro scale, and it was confirmed that 85% of the total turbulent kinetic energy in the flow was resolved.

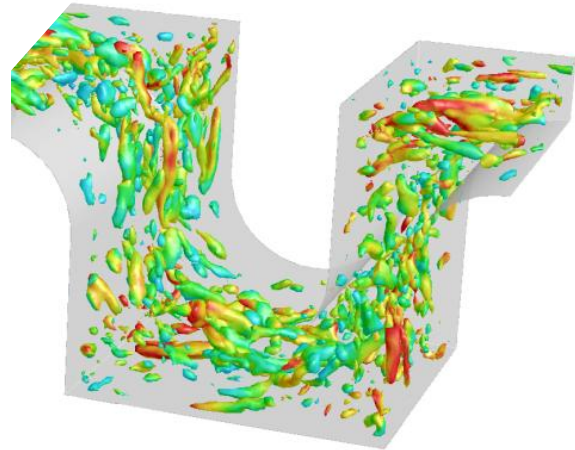


Figure 2: Turbulence structures visualized by vorticity magnitude, 0-3000 s⁻¹, coloured on iso-Q surfaces.

The grid resolution and the time step needed is not fully specified from a turbulence point of view, in addition the dispersed phase must be resolved accurately, particularly in the regions of large gradients of the secondary phase, i.e. regions of large gradients of the phase function C . In fact this requirement makes the simulation times rather long but running the simulations on a computer cluster compensate for this. In order to make the simulations efficient a dynamic grid refinement and coarsening is also used. This allows a dense grid only in regions where it is needed, as shown in Figure 3. In regions far from the dispersed phase, i.e. in the bulk, the restriction for large eddy simulations is determining the required grid resolution.

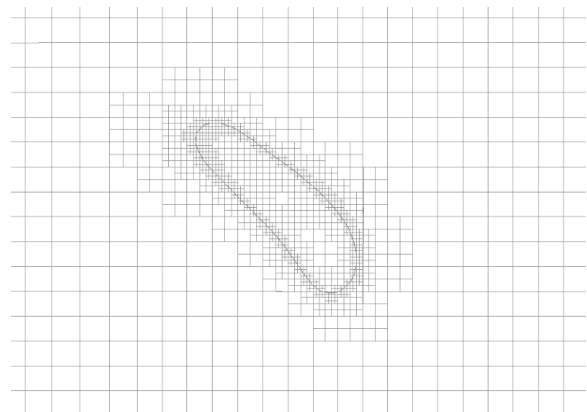


Figure 3: Dynamic multilevel grid refinement around and inside a deformed drop, immersed into a turbulent flow. The iso-line shows the phase function, $C=0.5$.

When the turbulent kinetic energy is transferred from the vortices to the fluid particles it results in deformation and stretching, as shown in Figure 4. Figure 4 shows the convection and small scale deformation of a fluid particle immersed into turbulent flow, here the small scale deformations occur over small time scales. As long as the stabilizing stresses are larger than the disruptive stresses the drops and bubbles will dissipate the surplus of

interfacial energy and re-attain its original spherical shape. Then this process starts all over again when the particle interact with a new vortex. The amplitude and frequency of the these deformations depends on what vortices it interacts with.

The normalized interfacial energy, defined by

$$\gamma(t) = \frac{\sigma A(t)}{\sigma A_0} = \frac{A(t)}{A_0} \quad (8)$$

quantifies how far from the thermodynamic stable spherical shape, A_0 , the fluid particles gets during its exposure to the turbulent flow field. These values obviously change in time as a result from the continuous interaction with vortices. The amplitude does depend on the ratio of the disruptive and stabilising stresses. Typical values observed during the non-disruptive stretching and deformation were within the range $1.00 < \gamma < 1.2$.

An important question is whether the sequential interaction with different vortices accumulate energy. In these simulations no indications of this was observed in the simulations. Based on analysis of the simulated data it seems that the amplitude keeps below the $\gamma < 1.2$ limit over several periods.

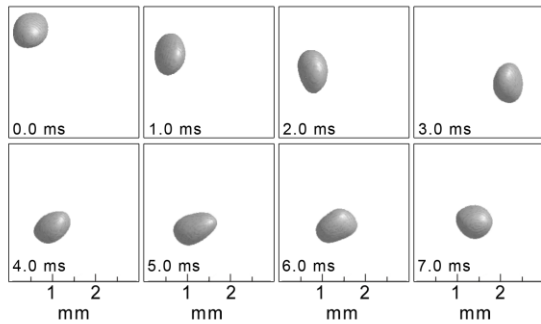


Figure 4: Small scale deformation of the fluid particle, caused by the continuous phase turbulent vortices. Here the fluid particle is visualized using iso-surfaces of the phase function $C=0.5$.

Contrary, the breakup events are characterized by significantly higher degree of deformation, typically in the range $1.3 < \gamma < 1.6$. The deformation originally starts from γ -values close to 1.0 and is followed by a rapid increase in interfacial area, as shown in Figure 5. Here the stretching is completed within approximately 7-8ms and breakup within 9ms.

Figure 5 also includes results from simulations where two different grid resolutions were used. It is concluded that regardless of the grid resolution used, i.e. level of dynamic grid adaption, the energy transfer rate is not significantly different. This conclusion holds for the intermediate and dense mesh, for which the grid size in the interfacial region is $1/25$ and $1/50$ of d_0 respectively, and can not be extrapolated.

Neither does the peak value close to 1.45 differ between these two resolutions. This means that the deformation and stretching occurs to the same extent. The observation that the energy increase before breakage is between 30%-60% agrees well with previous estimation

from experimental data and model development (Andersson and Andersson, 2006a).

Despite these similarities, there is one important feature which can not be identified in Figure 5. That is the formation of a small satellite drop between the two mother fragments. As shown in Figure 6 and Figure 7, there are two equally sized fragments formed with one small fragment in between (the satellite fragment is highlighted with an arrow in Figure 7). In this case the grid resolution needed to resolve the smallest satellite fragment is $1/50$ of d_0 , labelled 'dense grid' in Figure 5, and the resolution at the interface for intermediate grid corresponds to $1/25$ of d_0 .

As shown in the left column in Figure 6, the satellite fragment was also formed in the experiment. In fact the small satellite fragment contribute little to the overall interfacial area increase. Hence this effect can not be seen in Figure 5.

It can be concluded that the similarities between simulation and experiments are very good – not only with respect to the deformation degree and number of fragments formed, but also with respect to the deformation timescale. The deformation stretching and final breakage into fragments occurs in approximately 9ms also in the experiments. Hence the model prediction is in very good agreement with the measurements during the whole event. This allows and motivates further analysis of how the different turbulent structures interact and transfer energy.

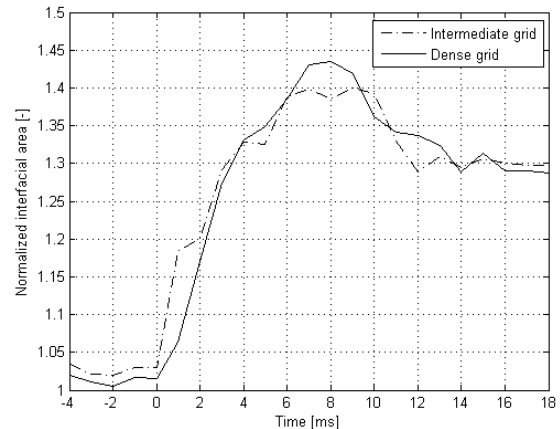


Figure 5: Comparison of normalized interfacial area during the breakup process, using two different grid resolutions.

This particular breakup event occurs by interaction with one strong vortex that transfers energy during its life time as seen in Figure 8. The interaction is between one vortex that is larger than the fluid particle. As seen in the figure, at this particular time the vortex has caused a significantly deformation and the particle starts to form a neck in the middle.

A more detailed view at Figure 8 also reveals that the principal axis of the vortex core and the axis of the deformed particle are not aligned in parallel. Instead they are rather perpendicular which is logical in that deformation is due to the vortex rotation.

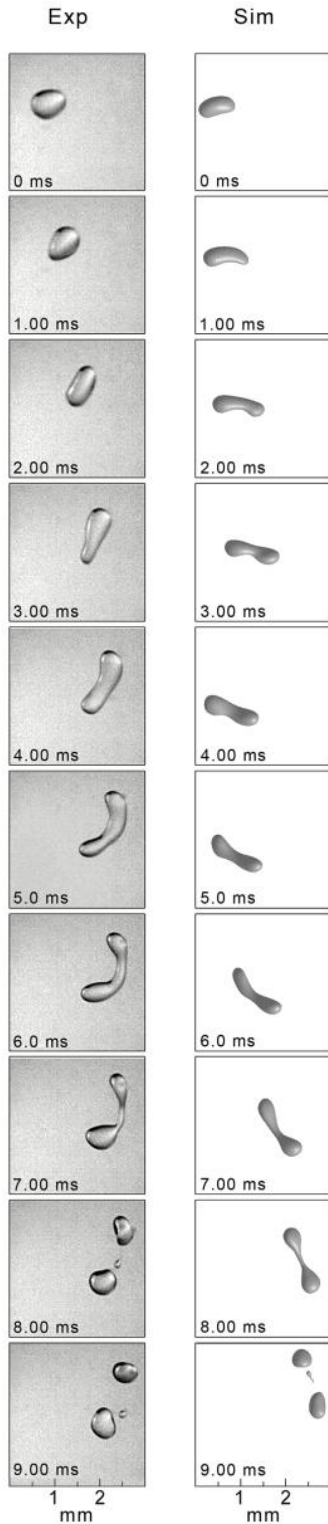


Figure 6: Dynamics of drop breakup, comparison between experimental measurement and simulation, $\epsilon=8.5 \text{ m}^2/\text{s}^3$. The left column is experimental measurements at 1 kHz, the right column is simulations using dense grid resolution at the interface i.e. $1/50$ of d_0 .

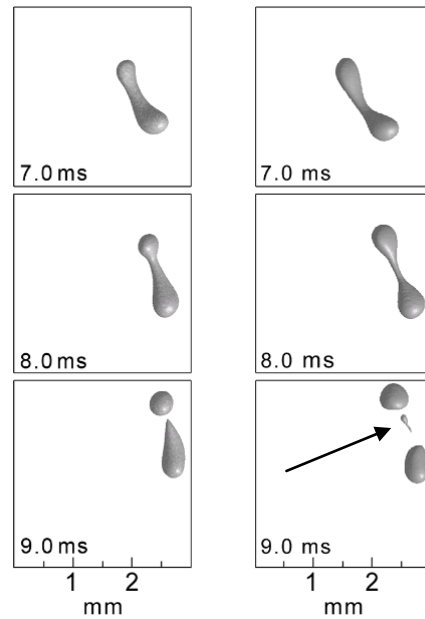


Figure 7: Comparison between a.) intermediate grid resolution $1/25$ of d_0 and b.) dense grid resolution $1/50$ of d_0 . The arrow in the lower right corner points at the satellite fragment.

Analysis of other data sets confirm similar deformation length scales, fragment sizes and breakup time scales. Interestingly this data also occasionally reveals events where two vortices, with their core axes aligned, simultaneously interact and deform the particle, as shown in Figure 9. In this figure it is clear that the two vortices are of different size. It is also seen that the vortex axes are aligned in parallel, and that the principal axis of the deformed particle is perpendicular to these vortex axes.

Further, the colour coding that is used i.e. vorticity component, reveals that the two vortices are rotating in different directions i.e. they are paired vortices.

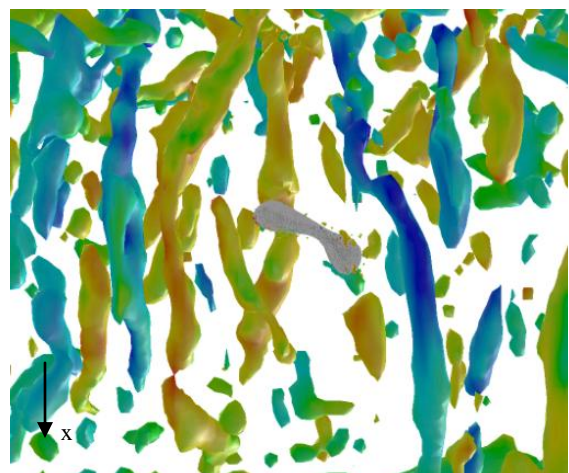


Figure 8: Fluid particle deformation and stretching due to interaction with a turbulent vortex. The drop (gray) is located in the middle of the figure. Here the x-vorticity, $-3000 - 3000 \text{ s}^{-1}$, is coloured on iso-Q surfaces.

When interaction occurs simultaneously with two or more vortices it will increase the probability for breakup and must be accounted for when developing new models for breakup. Too little data is currently available to quantify how frequent the interaction with two vortices is in relationship to interaction with one single vortex.

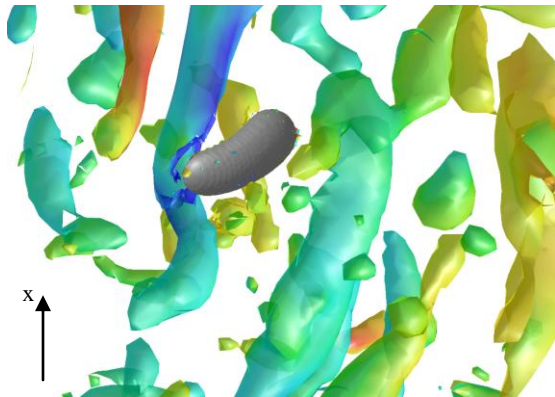


Figure 9: Two turbulent vortices stretching a fluid particle. Here the x-vorticity, $-3000 - 3000 \text{ s}^{-1}$, is coloured on the iso-Q surfaces. The vortices have their core axes aligned in parallel and the colour coding reveals that they are paired.

CONCLUSION

High-speed imaging of breakup of fluid particles in turbulent flows was used to validate combined LES and VOF simulations. Comparison with experiments show very good agreement with respect to deformation scale, breakup time, fragmentation pattern and daughter size distributions. By using the Q-criteria to identify the turbulent vortices, and analysis of the breakup dynamics it is revealed that eddies larger than the fluid particles also contribute to the breakup. This information is very valuable for future model development, particularly since some of the most popular models in the literature, now available in commercial CFD codes, are very sensitive the threshold value of the upper eddy size. The vortex core axis and the axis of the deformed fluid particle were frequently aligned perpendicularly to each other. It was also found that the breakup sometimes occurs due to interaction with more than one turbulent vortex at the same time. This means that more energy is available for the breakup and it will affect the breakup rate.

ACKNOWLEDGEMENTS

The simulations were done on the supercomputer cluster at Chalmers University of Technology and was supported by the Swedish National Infrastructure for Computing, SNIC.

REFERENCES

- ANDERSSON, R. and ANDERSSON, B. (2006a). "Modeling the breakup of fluid particles in turbulent flows". *AIChE Journal*, **52**, 2031-2038.
- ANDERSSON, R. and ANDERSSON, B. (2006b). "On the breakup of fluid particles in turbulent flows". *AIChE Journal*, **52**, 2020-2030.
- ANDERSSON, R., ANDERSSON, B., CHOPARD, F. and NOREN, T. (2004). "Development of a multi-scale simulation method for design of novel multiphase reactors". *Chemical Engineering Science*, **59**, 4911-4917.
- BOUAIFI, M., MORTENSEN, M., ANDERSSON, R., ORCIUCH, W. and ANDERSSON, B. (2004). "Experimental and numerical investigations of jet mixing in a multifunctional channel reactor: Passive and reactive systems". *Chemical Engineering Research and Design*, **82**, 274-283.
- BRACKBILL, J. U., KOTHE, D. B. and ZEMACH, C. (1992). "A continuum method for modelling surface tension". *Journal of Computational Physics*, **100**, 335-354.
- HUNT, J. C. R. (1987). "Vorticity and vortex dynamics in complex turbulent flows". *Transactions of the Canadian Society for Mechanical Engineering*, **11**, 21-35.
- LACANETTE, D., GOSSET, A., VINCENT, S., BUCHLIN, J. M. and ARQUIS, E. (2006). "Macroscopic analysis of gas-jet wiping: Numerical simulation and experimental approach". *Physics of fluids*, **18**.
- LI, J., RENARDY, Y. Y. and RENARDY, M. (2000). "Numerical simulation of breakup of a viscous drop in simple shear flow through a volume-of-fluid method". *Physics of fluids*, **12**, 269-282.
- LIAO, Y. X. and LUCAS, D. (2009). "A literature review of theoretical models for drop and bubble breakup in turbulent dispersions". *Chemical Engineering Science*, **64**, 3389-3406.
- LIAO, Y. X. and LUCAS, D. (2010). "A literature review on mechanisms and models for the coalescence process of fluid particles". *Chemical Engineering Science*, **65**, 2851-2864.
- LILLY, D. K. (1992). "A proposed modification of the germano-subgrid-scale closure method". *Physics of Fluids*, **4**, 633-635.
- LUBIN, P., VINCENT, S., ABADIE, S. and CALTAGIRONE, J.-P. (2006). "Three-dimensional Large Eddy Simulation of air entrainment under plunging breaking waves". *Coastal Engineering*, **53**, 631-655.
- SHINJO, J. and UMEMURA, A. (2010). "Simulation of liquid jet primary breakup: Dynamics of ligament and droplet formation". *International Journal of Multiphase Flow*, **36**, 513-532.